AIAA AVIATION Forum
June 15-19, 2020, VIRTUAL EVENT
AIAA AVIATION 2020 FORUM

10.2514/6.2020-2942

Investigation of Coflow Jet Active Flow Control for Wind Turbine Airfoil

Kewei Xu *, Gecheng Zha †
Dept. of Mechanical and Aerospace Engineering
University of Miami, Coral Gables, Florida 33124
E-mail: gzha@miami.edu

Abstract

This paper applies Co-flow Jet (CFJ) active flow control (AFC) to the wind turbine S809 airfoil to optimize the CFJ-S809 airfoil with significant lift coefficient increase at low energy expenditure. The effects of injection slot-size, injection slot location, suction slot-size and suction slot location are studied. The high fidelity in-house CFD code FASIP with two-equation k-ω shear stress transport (SST) turbulence model is utilized to better predict flow separation. The 2D Unsteady Reynolds averaged Navier-Stokes (URANS) equations are used for high angle of attack simulations to accurately capture flow unsteadiness. Steady state RANS is used for low angle of attack simulations. The baseline S809 airfoil is validated with experiment. The predicted lift coefficient (C_L) and drag coefficient (C_D) achieve a good agreement with experiment except a slight deviation at very high or very low angle of attack (AoA) due to flow separation. The predicted airfoil surface pressure coefficient distribution (C_p) at various AoA also agrees well with experiment. The CFJ-S809 airfoil is simulated with three injection total pressure of 1.01, 1.02 and 1.03 (Pt_{inj}, normalized by free-stream static pressure), which corresponds to the C_μ varying from 0.02 to 0.09. A small Pt_{inj} of 1.01 is able to increase C_{Lmax} over 45%. The suction location study indicates that suction slot located at the geometry inflection point at 53%C is the optimum due to it's efficiency and effectiveness to suppress airfoil stall at high AoA. The suction slot-size of 1.0%C is adopted since it decelerates the flow well with little flow separation inside the suction duct. For the injection slot-size, the 0.75%C slot-size minimizes the power coefficients by reducing the required injection total pressure, and therefore is the optimum. The injection location of 3%C is the optimum due to it's better energy efficiency at high angle attack. Compared with the baseline S809 airfoil, the optimum configuration is able to increase C_{Lmax} by 42.3% with a similar amount or higher $(C_L/C_D)_c$.

Nomenclature

AoA	Angle of attack
AFC	Active Flow Control
C	Chord length
CFJ	Co-flow jet
C_L	Lift coefficient
C_D	Drag coefficient
C_p	Constant pressure specific heat
C_μ	Jet momentum coefficient $\dot{m}_j U_j/(q_\infty S)$

* Ph.D. Candidate
† Professor, AIAA associate Fellow

C_L/C_D	Aerodynamic efficiency
$(C_L/C_D)_c$	Aerodynamic efficiency corrected for CFJ airfoil
D	Total drag on the airfoil
$FASIP$	Flow-Acoustics-Structure Interaction Package
H_t	Total enthalpy
L	Total lift on the airfoil
LE	Leading Edge
$\dot{m}$	Mass flow rate
M	Mach number
MAC	mean aerodynamic chord
P	CFJ Pumping power
P_c	Power coefficient, $P_c = \frac{P}{\frac{1}{2}\rho_\infty V_\infty^3 S}$
p_t	Total pressure at injection duct inlet
Pt_{inj}	Injection total pressure
Ptr	Total pressure ratio of CFJ micro-compressor
$RANS$	Reynolds-Averaged Navier-Stokes
R_e	Reynolds number
TE	Trailing Edge
T_t	Total temperature
$ZNMF$	Zero-Net Mass Flux
c	Subscript, stands for corrected
j	Subscript, stands for jet
γ	Air specific heats ratio
η	CFJ micro-compressor efficiency
θ_1	Angle between the injection slot surface and a line normal to the airfoil chord
θ_2	Angle between the suction slot surface and a line normal to the airfoil chord
∞	Freestream condition

1 Introduction

Wind turbine market is growing rapidly world wide for generating sustainable energy to combat global warming. The S809 airfoil is specially designed for horizontal axis wind turbine applications [1, 2], which can achieve a desirable lift coefficient and low profile-drag. However, an issue limiting wind turbine operation and life span is the blade stall caused by large scale unsteadiness of incoming flow. The other issue is that the power output efficiency of wind turbines are still low in general, in particular considering a range of wind speed and incoming flow incidence. Active flow control developed recently is not just able to significantly extend the range of wind turbine operation with mitigated stall, but also has great potential to increase power output efficiency.

Wang et.al [3] applied unsteady blowing jet on wind turbine airfoil and observed that the lift fluctuation is reduced with and without large scale unsteadiness in the freestream. Steady blowing jet [4] was also tested on S809 airfoil and achieved an improvement of maximum lift and stall delay. However, these studies of the blowing jet active flow control do not address how to provide the mass flow for blowing on the wind turbine systems. Maldonado et.al [5] implemented the zero-net-mass-flux synthetic jet on S809 wind turbine airfoil for dynamic stall conditions. Enhancement of flow reattachment is achieved for

pitch down and pitch up motion with angle of attack (AoA) of 15°. Gul [6] experimentally studied the effect of periodic excitation on the synthetic jet for removing flow separation of S809 airfoil. Driven with a sinusoidal frequency of 1.45 kHz and 300Vp-p, the periodic excitation from the synthetic jet actuators are able to eliminate the laminar separation bubble at zero angle of attack.

Recently, a zero-net-mass-flux (ZNMF) co-flow jet (CFJ) AFC shows a great promise to enhance airfoil performance by achieving ultra-high lift coefficient at very high stall angle of attack (e.g. 70°) and high aerodynamic efficiency at low angle of attack with low energy expenditure [7, 8, 9, 10, 11, 12, 13, 14, 15, 16, 17, 18, 19, 20, 21, 22]. As sketched in Fig. 1, a CFJ airfoil draws a small amount of mass flow into the airfoil near the trailing edge, pressurizes and energizes it using a micro-compressor embedded inside the airfoil, and then tangentially injects the mass flow near the leading edge in the main flow direction. The whole process does not add any mass flow to the system and hence is a ZNMF flow control.

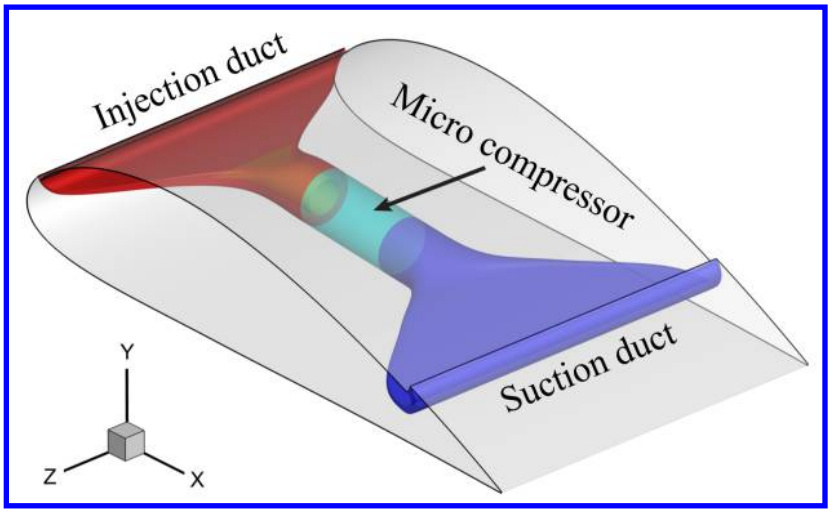

Figure 1: Schematics of CFJ wing.

Co-flow jet is applied to S809 airfoil in previous studies [23, 24], which is focused on understanding the co-flow jet effect on suppressing the dynamic stall. This paper is to conduct trade study of the CFJ-S809 airfoil to understand the parametric effect on the airfoil performance in order to achieve the optimum design. The studied parameters include injection jet strength controlled by the injection total pressure, injection slot-size, injection slot location, suction slot-size and suction slot location.

2 CFJ Parameters

This section lists the important parameters used to evaluate aerodynamic performance of a CFJ airfoil.

2.1 Jet Momentum Coefficient

The jet momentum coefficient C_μ is a parameter used to quantify the jet intensity. It is defined as:

$$C_\mu = \frac{\dot{m} V_j}{\frac{1}{2}\rho_\infty {V_\infty}^2 S} \tag{1}$$

where $\dot{m}$ is the injection mass flow, V_j is the mass-averaged injection velocity, ρ_∞ and V_∞ denote the free stream density and velocity, and S is the planform area.

2.2 Lift and Drag Calculation

For CFD simulation, the full reactionary forces produced by the momentum and pressure at the injection and suction slots are included by using control volume analysis. Zha et al. [9] gives the following formulations to calculate the lift and drag due to the jet reactionary force for a CFJ airfoil. By considering the effects of injection and suction jets on the CFJ airfoil, the expressions for these reactionary forces are given as:

$$F_{x_{cfj}} = (\dot{m}_j V_{j1} + p_{j1} A_{j1}) * cos(\theta_1 - \alpha) - (\dot{m}_j V_{j2} + p_{j2} A_{j2}) * cos(\theta_2 + \alpha) \tag{2}$$

$$F_{y_{cfj}} = (\dot{m}_{j1} V_{j1} + p_{j1} A_{j1}) * sin(\theta_1 - \alpha) + (\dot{m}_{j2} V_{j2} + p_{j2} A_{j2}) * sin(\theta_2 + \alpha) \tag{3}$$

where the subscripts 1 and 2 stand for the injection and suction respectively, and θ_1 and θ_2 are the angles between the injection and suction slot's surface and a line normal to the airfoil chord. α is the angle of attack.

The total lift and drag on the airfoil can then be expressed as:

$$D = R'_x - F_{x_{cfj}} \tag{4}$$

$$L = R'_y - F_{y_{cfj}} \tag{5}$$

where R'_x and R'_y are the surface integral of pressure and shear stress in x (drag) and y (lift) direction excluding the internal ducts of injection and suction. For CFJ wing simulations, the total lift and drag are calculated by integrating Eqs.(4) and (5) in the spanwise direction.

2.3 Power Coefficient

The power consumption is determined by the jet mass flow and total enthalpy change as the following:

$$P = \dot{m}(H_{t1} - H_{t2}) \tag{6}$$

where H_{t1} and H_{t2} are the mass-averaged total enthalpy in the injection cavity and suction cavity respectively, P is the power required by the pump and $\dot{m}$ the jet mass flow rate. Introducing p_{t1} and p_{t2} as the mass-averaged total pressure in the injection and suction cavity respectively, the pump efficiency η, and the total pressure ratio of the pump $Ptr = \frac{p_{t1}}{p_{t2}}$, the power consumption is expressed as:

$$P = \frac{\dot{m} C_p T_{t2}}{\eta} (Ptr^{\frac{\gamma-1}{\gamma}} - 1) \tag{7}$$

where γ is the specific heat ratio equal to 1.4 for air. The power coefficient is expressed as:

$$P_c = \frac{P}{\frac{1}{2}\rho_\infty V_\infty^3 S} \tag{8}$$

2.4 Corrected Aerodynamic Efficiency

The conventional wing aerodynamic efficiency is defined as:

$$\frac{L}{D} \tag{9}$$

For the CFJ wing, the ratio above still represents the pure aerodynamic relationship between lift and drag. However, since CFJ active flow control consumes energy, the ratio above is modified to take into account the energy consumption of the pump. The formulation of the corrected aerodynamic efficiency for CFJ wings is:

$$(\frac{L}{D})_c = \frac{C_L}{C_D + P_c} \tag{10}$$

where P_c is the power coefficient, L and D are the lift and drag generated by the CFJ wing. The formulation above converts the power consumed by the CFJ into a force $\frac{P}{V_\infty}$ which is added to the aerodynamic drag D. If the pumping power is set to 0, this formulation returns to the aerodynamic efficiency of a conventional wing.

3 The Numerical Algorithm

The in-house high order accuracy CFD code Flow-Acoustics-Structure Interaction Package (FASIP) is used to conduct the numerical simulation. 2D steady state Reynolds averaged Navier-Stokes (RANS) equations are used to simulate the low AoA conditions. Once AoA is greater than 20°, the Unsteady Reynolds averaged Navier-Stokes (URANS) equations are used to capture the unsteadiness. Two-equation k-ω shear stress transport (SST) turbulence model [25] is used for the turbulence modeling. A 3rd order WENO scheme for the inviscid flux [26, 27, 28] and a 2nd order central differencing for the viscous terms are employed to discretize the Navier-Stokes equations. The Roe's Riemann solver is utilized with the WENO scheme to evaluate the inviscid fluxes. Implicit time marching method using Gauss-Seidel line relaxation is used to achieve a fast convergence rate [29]. Parallel computing is implemented to save wall clock simulation time [30]. The FASIP code is intensively validated for CFJ airfoil simulations [8, 9, 10, 11, 14, 15, 16, 31, 32, 33]. The unsteady numerical results are presented after the flow and all the aerodynamic forces become statistically stable.

4 Validation of Baseline S809 Airfoil

Fig. 2 shows the geometry of S809 airfoil with the CFD mesh around the airfoil used for this study. The airfoil has the maximum thickness of 21-percent chord. It is experimentally tested in [1, 2] with freestream Ma_∞=0.076 and freestream Re_∞=1.0×10^6. The experimental test conditions are used for the simulation. The boundary conditions setup for the far-field are the total pressure, total temperature and flow angle at the inlet and static pressure outlet. Non-slip wall boundary condition is applied on the airfoil and CFJ ducts surfaces. For the CFJ duct boundary conditions, the injection duct inlet has the specified total pressure, total temperature and flow angle, and the suction duct outlet has the static pressure specified.

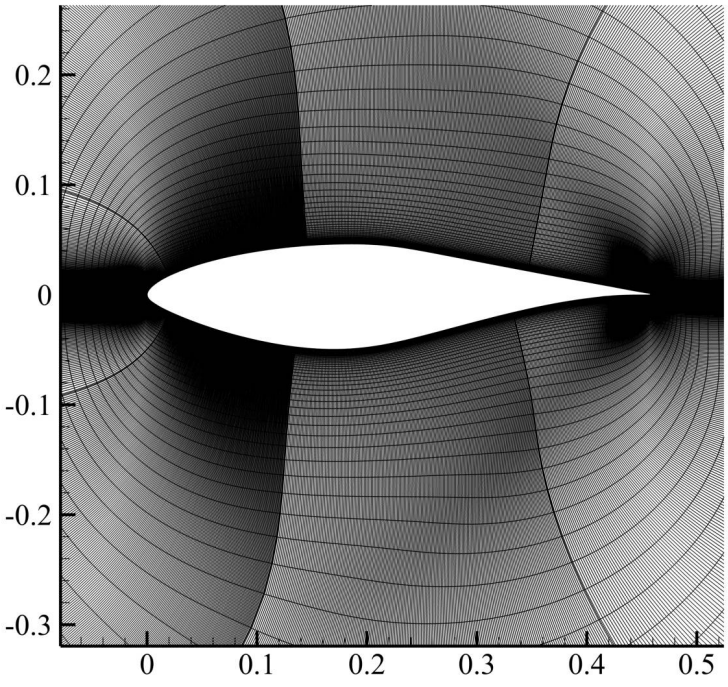

Figure 2: Baseline S809 airfoil.

The baseline S809 airfoil is meshed using a refined structured O-grid with 0.1694 million points. Details of the mesh dimensions and spacing are presented in Table.1. The first layer spacing is 1×10^{-5} to ensure y$^+$ less than 1.

Table 1: Grid Details

Parameters	S809 mesh
Radius of far field	50 C
Normal layers in mesh	120
Wrap-around points	1400
Spacing growth ratio	1.13
Total number of points	1.7×10^5

Fig. 3 shows the comparison of the predicted lift coefficient (C_L) and drag coefficient (C_D) with the experiment versus angle of attack (AoA). Overall, a very good agreement between the numerical simulation and experiment is obtained. Both the lift and drag coefficients are slightly over-predicted at the high AoA range when the flow is stalled with separation. The simulation is further validated by comparing the pressure coefficient C_p distributions with the experiment as shown in Fig. 4. Again, the CFD simulation achieves a good agreement with the experiments for AoA of 0°, 6.1°, and 18.1°. For the very high AoA of 24°, the suction surface flow is massively separated and the predicted C_p is a little offset from the experiment.

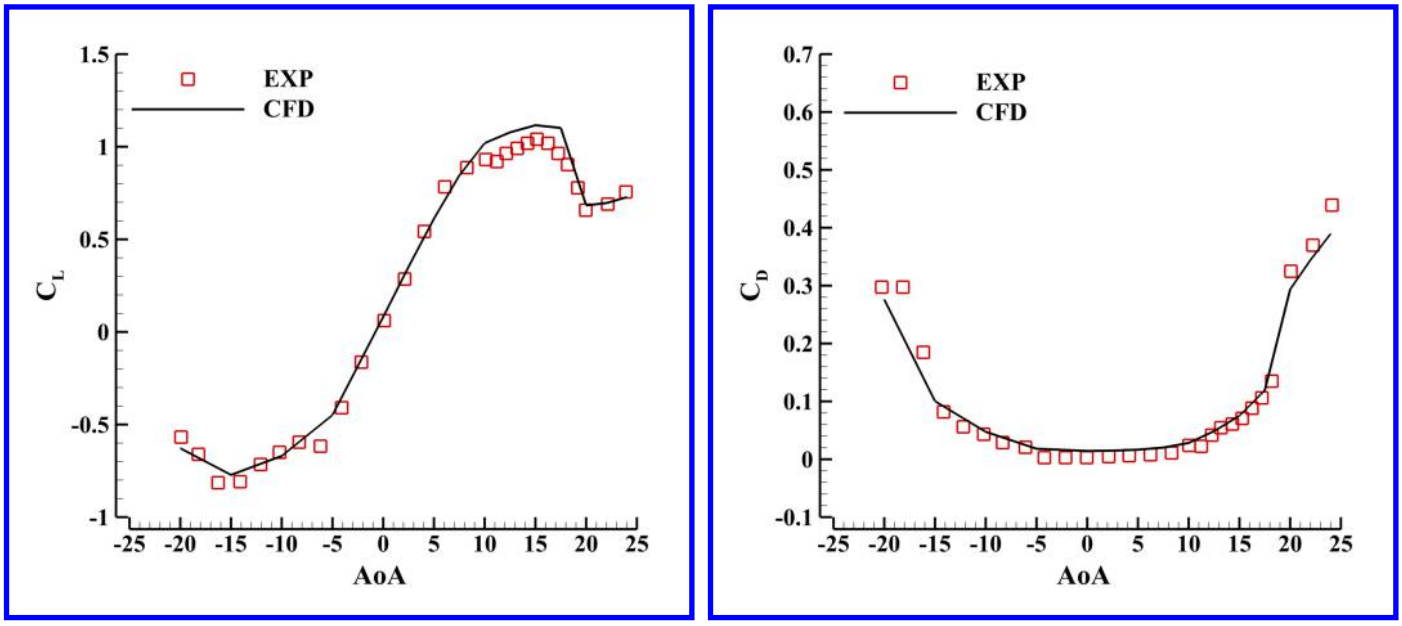

(a) Lift coefficient (b) Drag coefficient

Figure 3: Comparison of predicted aerodynamic coefficients with experiments

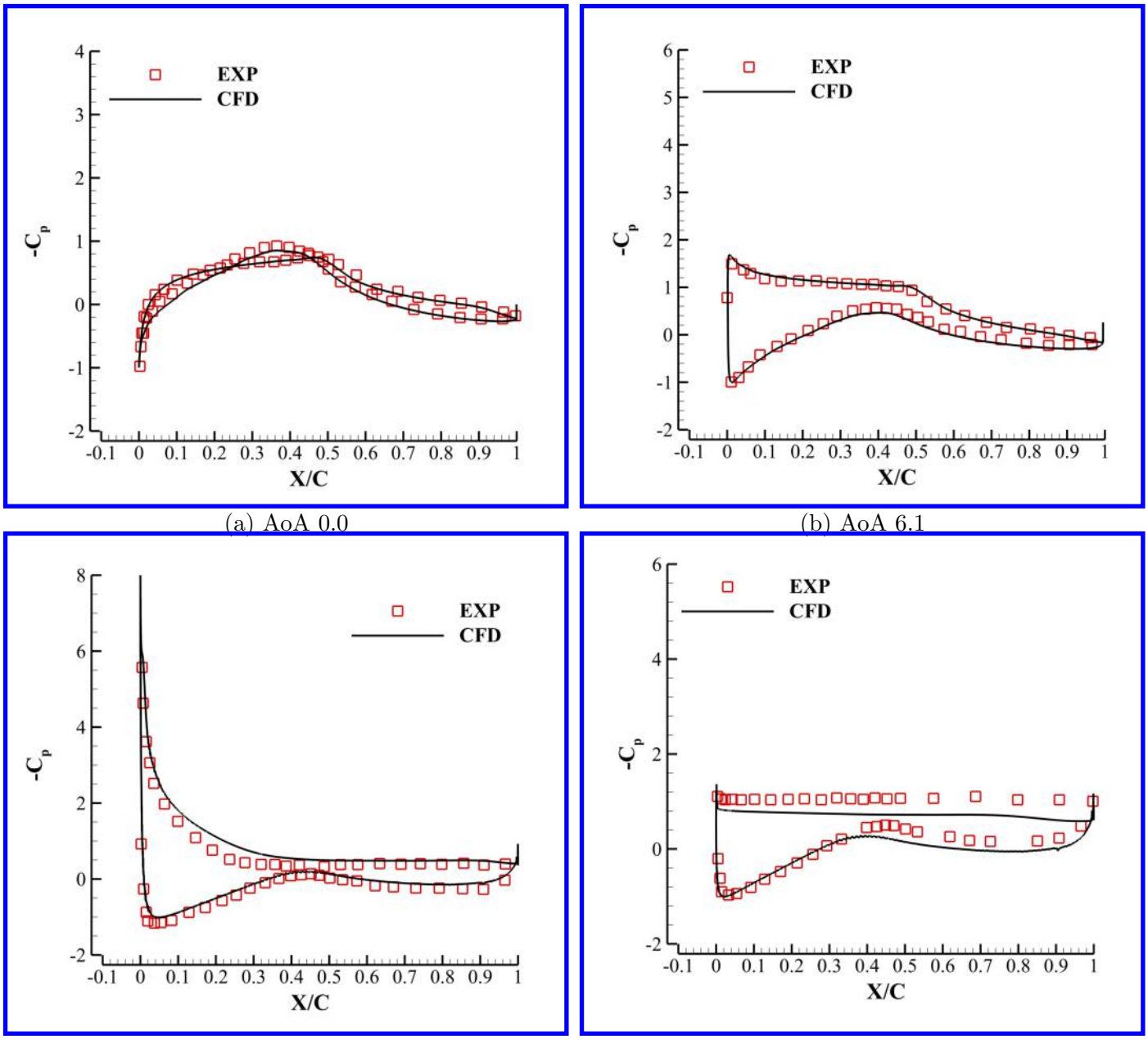

(a) AoA 0.0 (b) AoA 6.1

(c) AoA 18.1 (d) AoA 24.0

Figure 4: Comparison of C_p distributions between simulations and experiments

5 CFJ Results

The results of the parametric trade study on suction location, suction slot-size, injection location and injection slot-size are presented in this section. Before the parametric studies, three injection total pressure (Pt_{inj}, normalized by the free-stream static pressure) of 1.01, 1.02 and 1.03 are used to investigate the performance improvement with respect to different energy input of Co-flow Jet. The optimum configuration is determined based on the C_L enhancement, power consumption (P_c) and corrected aerodynamic efficiency

$((C_L/C_D)_c)$.

5.1 Co-Flow Jet S809 Airfoil

As sketched in Fig. 5, the CFJ-S809 airfoil is created based on the baseline S809 airfoil by adding the injection duct (in blue) near leading edge and suction duct (in red) after mid-chord.

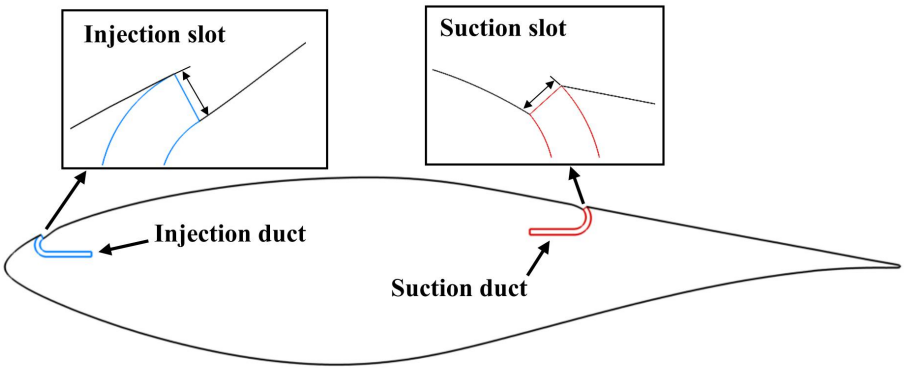

Figure 5: Schematics of the CFJ-S809 airfoil.

5.2 Injection Total Pressure Effect

The injection total pressure will determine the injection momentum coefficient. The variation of the injection total pressure is to vary the injection momentum coefficient. For this injection momentum coefficient study, the CFJ-S809 airfoil has the injection slot located at 4%C with a size of 0.5%C and the suction location at 53%C and a size of 0.5%C. Three injection total pressure (Pt_{inj}) are studied with the corresponding C_μ varying from 0.01 to 0.09 as shown in Fig. 6. Even though the injection total pressure is only 1% to 3% higher than the free-stream static pressure, it is substantially higher than the local main flow static pressure at the injection slot area because the flow experiences a strong acceleration around the leading edge. Fig. 7 presents the aerodynamic coefficients of the baseline and the CFJ airfoil with different Pt_{inj}. With a small injection total pressure of 1.01 as shown in Fig. 7, C_L is increased about 80% at AoA 0° and C_{Lmax} is increased from 1.11 to 1.61, more than 45% increase compared with the baseline. Even though there is an enormous increase of C_L/C_D, the $(C_L/C_D)_c$ has a reduction of 29% due to the power consumed by CFJ. For the low injection Pt_{inj} of 1.01, at high AoA of 12.5° and 15°, both C_L and $(C_L/C_D)_c$ are substantially higher than those of the baseline as shown in Fig. 7 (a) and Fig. 7 (d). This indicates that with a small injection Pt_{inj} and momentum coefficient, the CFJ-S809 airfoil can not only achieve the significant improvement of C_L, but also has higher energy efficiency in high angle of attack operation. Increasing CFJ injection Pt_{inj} to 1.03, the C_{Lmax} is only increased by 15.6% compared with Pt_{inj} of 1.01. However, the power coefficient is increased dramatically from 0.053 to 0.153, almost three times, which decreases the corrected aerodynamic efficiency by 45%. This means that a high injection total pressure with a large power consumption is not desirable. Therefore, the small injection total pressure of 1.01 is utilized for the rest of the studies.

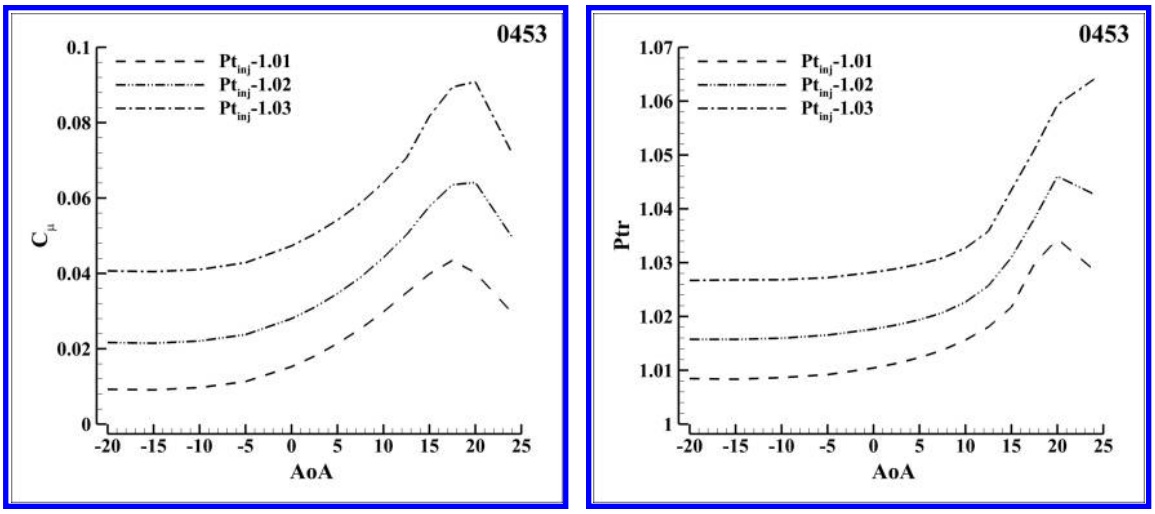

(a) Momentum coefficient C_μ (b) CFJ Total pressure ratio Ptr

Figure 6: C_μ and Ptr variations with AoA for three injection total pressure.

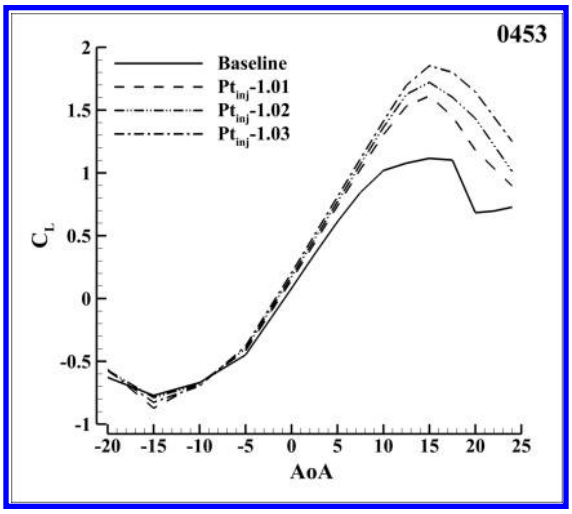

(a) Lift coefficient C_L

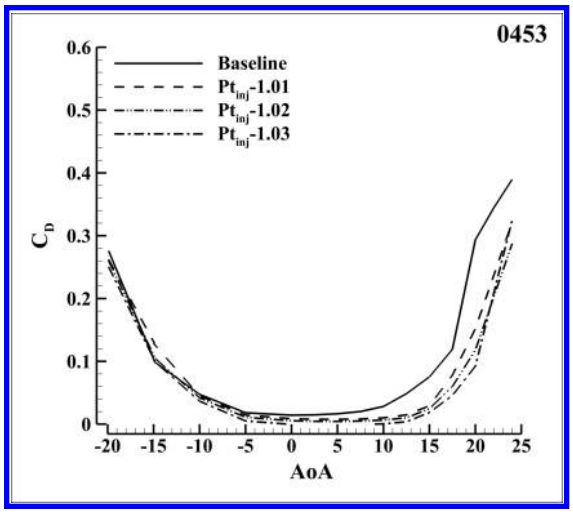

(b) Drag coefficient C_D

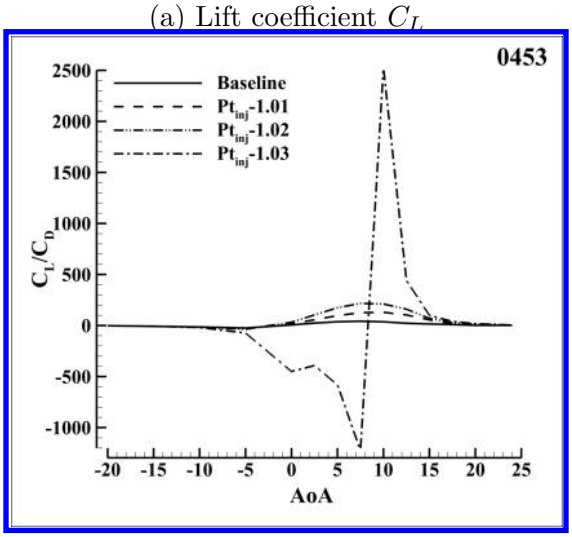

(c) Aerodynamic efficiency C_L/C_D

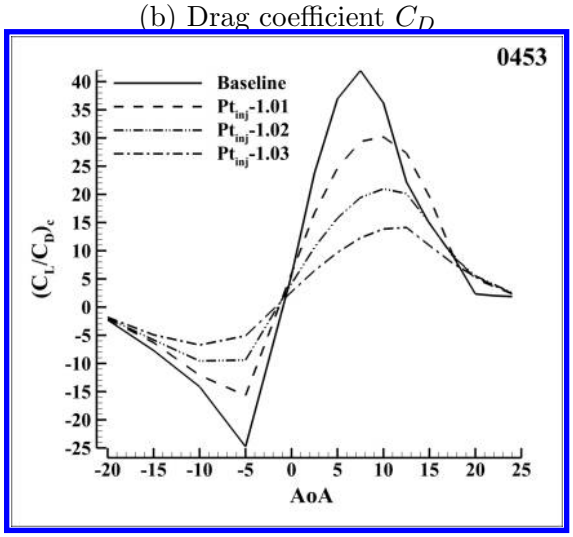

(d) Corrected aerodynamic efficiency $(C_L/C_D)_c$

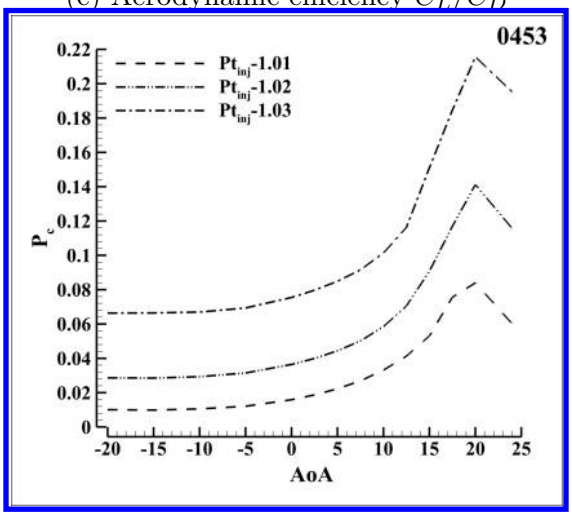

(e) Power coefficient P_c

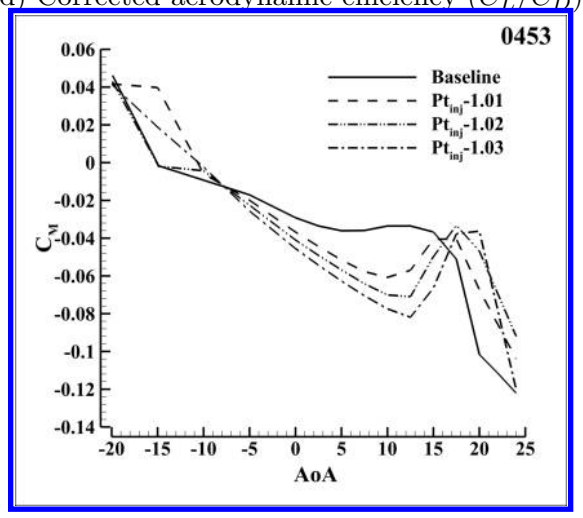

(f) Moment coefficient C_M

Figure 7: Aerodynamic coefficients of baseline and CFJ-S809 airfoils with injection Pt_{inj} variations.

5.3 Suction Location Study

The trade study starts with the initial configuration with the injection slot located at 4%C, a size of 0.5%C and the suction slot located at 65% with a size of 0.5%C. The CFJ-S809 airfoil has the suction location studied at 53%C, 65%C and 80%C. Fig. 8 presents the C_μ and Ptr variations with AoA for the three configurations at the fixed injection total pressure of 1.01. Other aerodynamic coefficients are presented in Fig. 9. A similar C_{Lmax} increase is achieved for all the three suction locations of 53%C, 65%C and 80%C. The 4-digit legends in Fig. 8 and Fig. 9 is to represent the injection location by the first 2 digits and the suction location by the last 2 digits. For example, 0453 means that the injection is at the 4%C location and the suction is at 53% chord location. As shown in Fig. 9 (e), the suction at 53%C has the minimum power consumption, which significantly increases $(C_L/C_D)_c$. At AoA of 15°, the suction at 53%C has a $(C_L/C_D)_c$ of 26.6% and 80.0% higher than the suction at 65%C and 80%C respectively. This is because 53%C is at the minimum slope extremum of the S809 suction surface as shown in Fig. 10. The 53%C position is the inflection point and generates the local maximum adverse pressure gradient (APG). Fig. 11 (b) compares the Mach number contours and streamlines of the baseline airfoil and the three CFJ airfoils with different suction locations. The flow separation onset of the baseline airfoil occurs at about 53%C location. It appears that placing the suction at the inflection point is most effective to energize the boundary layer and prevent separation onset. This is consistent with the findings in the previous study applying CFJ to NASA hump [21]. The 65%C and 80%C suction locations are inside the baseline airfoil flow separation zone, which deteriorates the boundary layer due to the high diffusion effect and increases the power consumption as illustrated in Fig. 11 (c) and (d). Even though the suction at 65%C can also fully attach the flow, the required P_C is 20.8% higher than that of the suction located at 53%C. Overall, the 53%C is the optimal suction location and is adopted for the following parametric studies.

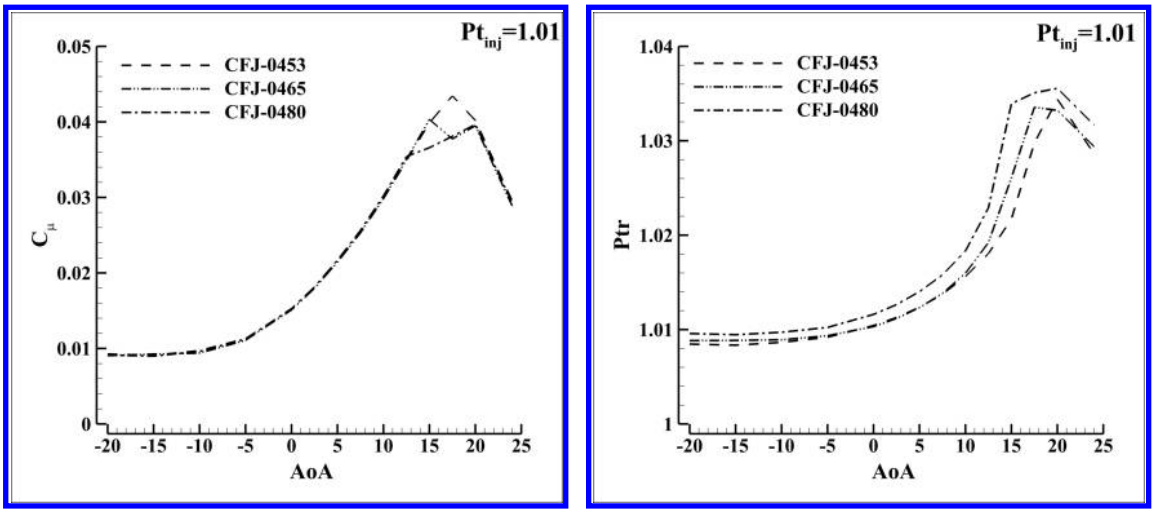

(a) Momentum coefficient C_μ (b) CFJ Total pressure ratio Ptr

Figure 8: C_μ and Ptr variations with AoA for suction location studies.

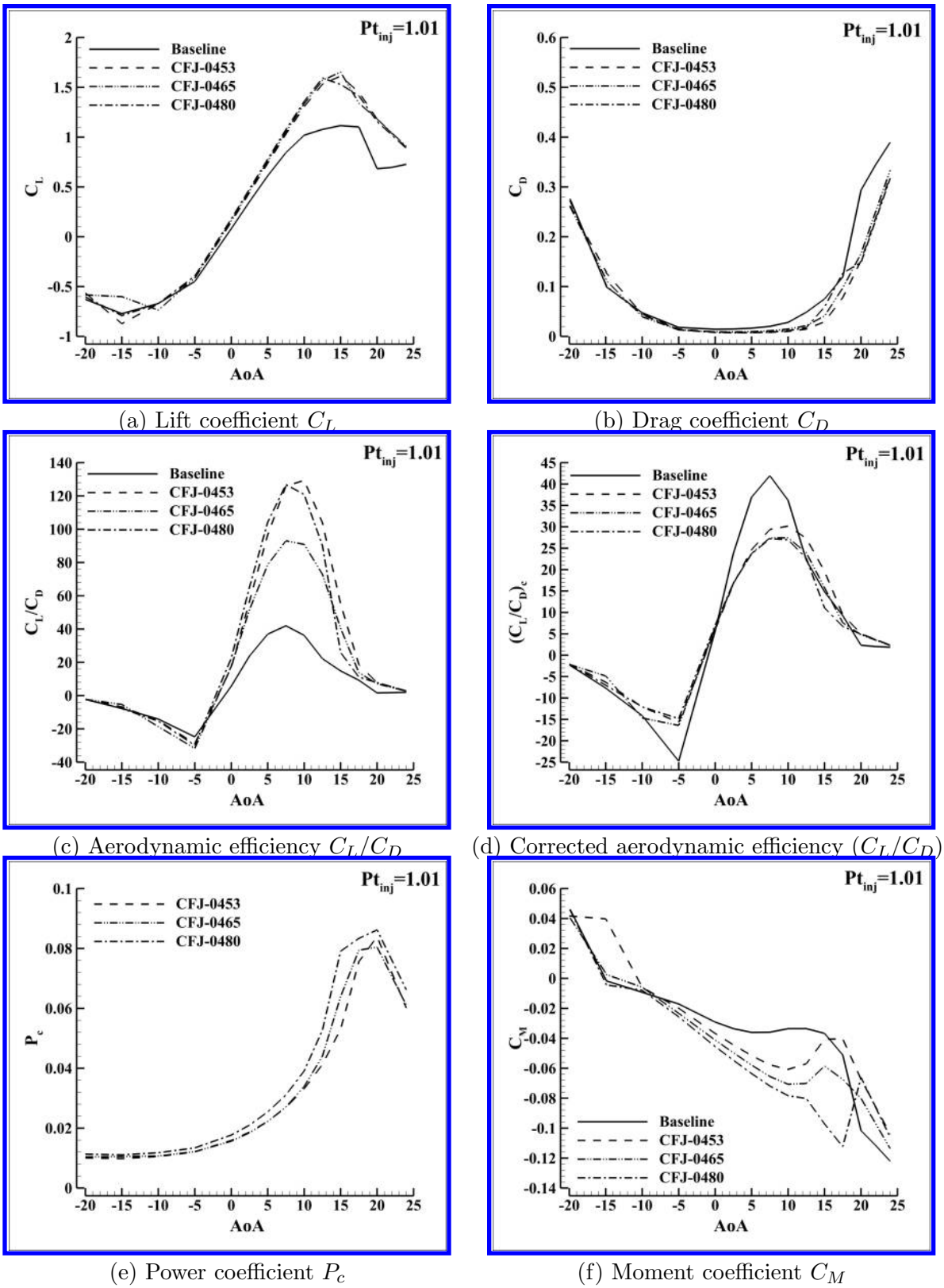

(a) Lift coefficient C_L

(b) Drag coefficient C_D

(c) Aerodynamic efficiency C_L/C_D

(d) Corrected aerodynamic efficiency $(C_L/C_D)_c$

(e) Power coefficient P_c

(f) Moment coefficient C_M

Figure 9: Aerodynamic coefficients of baseline and CFJ-S809 airfoils with suction slot location variations for Pt_{inj}=1.01.

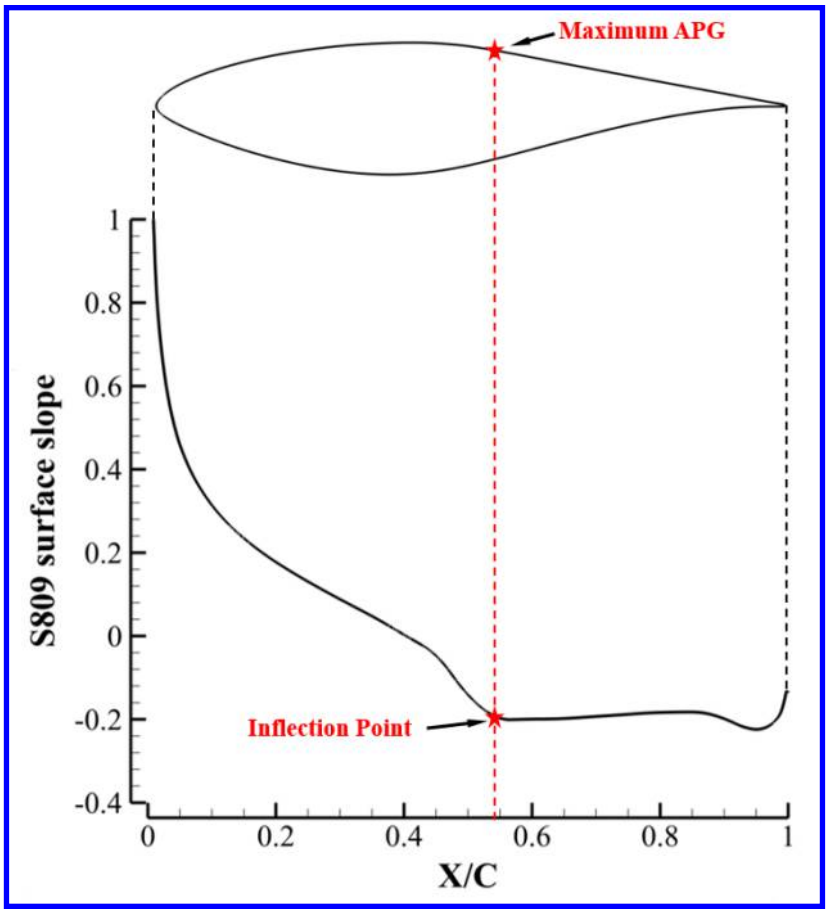

Figure 10: Baseline S809 airfoil slope distribution.

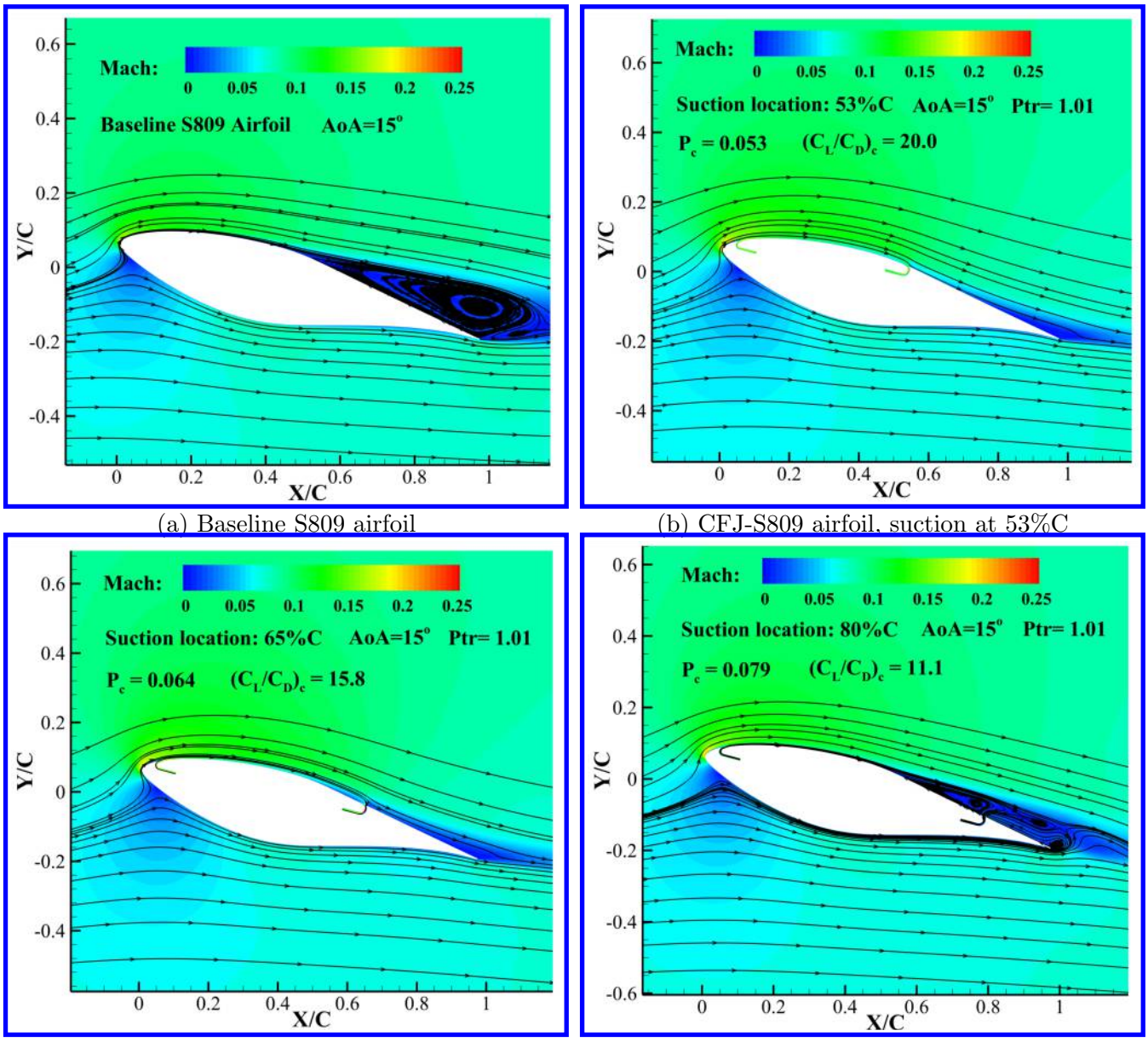

(a) Baseline S809 airfoil

(b) CFJ-S809 airfoil, suction at 53%C

(c) CFJ-S809 airfoil, suction at 65%C

(d) CFJ-S809 airfoil, suction at 80%C

Figure 11: Mach contours of the baseline and CFJ-S809 airfoils

5.4 Suction Slot-size Study

Fig. 13 presents the aerodynamic coefficients of the CFJ-S809 airfoils with suction slot-size of 0.5%C, 0.75%C and 1.0%C. The injection location and suction location is fixed at 4%C and 53%C, respectively. The injection slot-size is held at 0.5%C. As the suction slot-size is varied, the suction duct area is also changed to keep a constant channel area. Increasing the suction slot-size from 0.5%C to 1.0%C, the C_L, C_D, and C_M have small variation for the three configurations, but the C_L/C_D, $(C_L/C_D)_c$ and P_c have large variation for their peak values. The peak power coefficient (P_c) is reduced by 37.5% as suction slot-size is increased from 0.5%C to 1.0%C, which increases the maximum $(C_L/C_D)_c$ by 23.3%. The reduction of

power consumption benefits from the large duct area with lower velocity and energy loss. The peak C_L/C_D of the smallest suction slot-size of 0.5%C is a little higher than that of the larger slot size because the smaller suction slot-size has higher velocity to withdraw the same amount of the mass flow rate. Since the suction slot-size of 1.0%C achieves the highest $(C_L/C_D)_c$ with the minimum power consumption, it is adopted as the optimum size for the injection configuration studies.

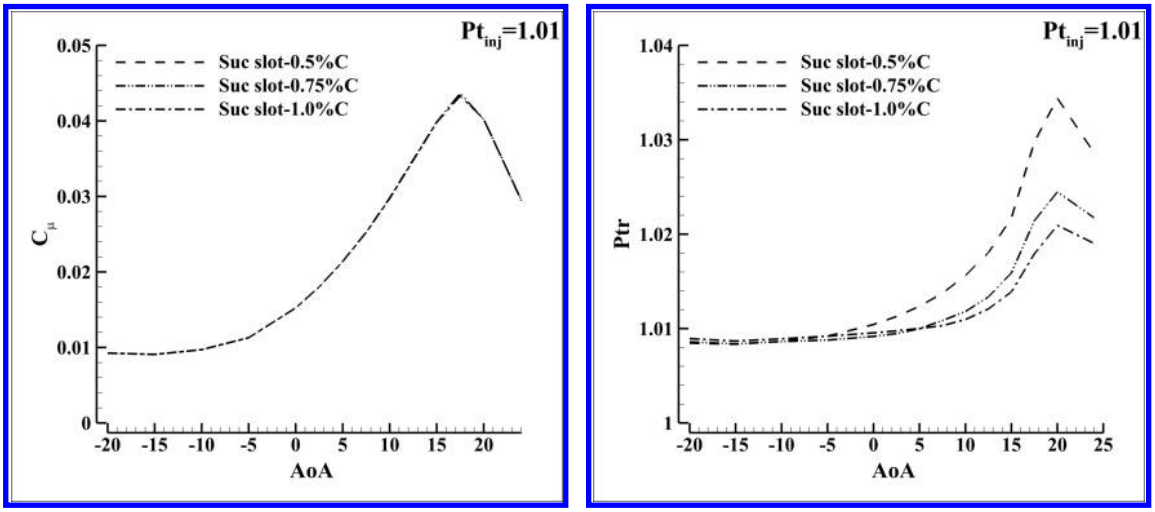

(a) Momentum coefficient C_μ (b) CFJ Total pressure ratio Ptr

Figure 12: C_μ and Ptr variations with AoA for suction slot-size studies.

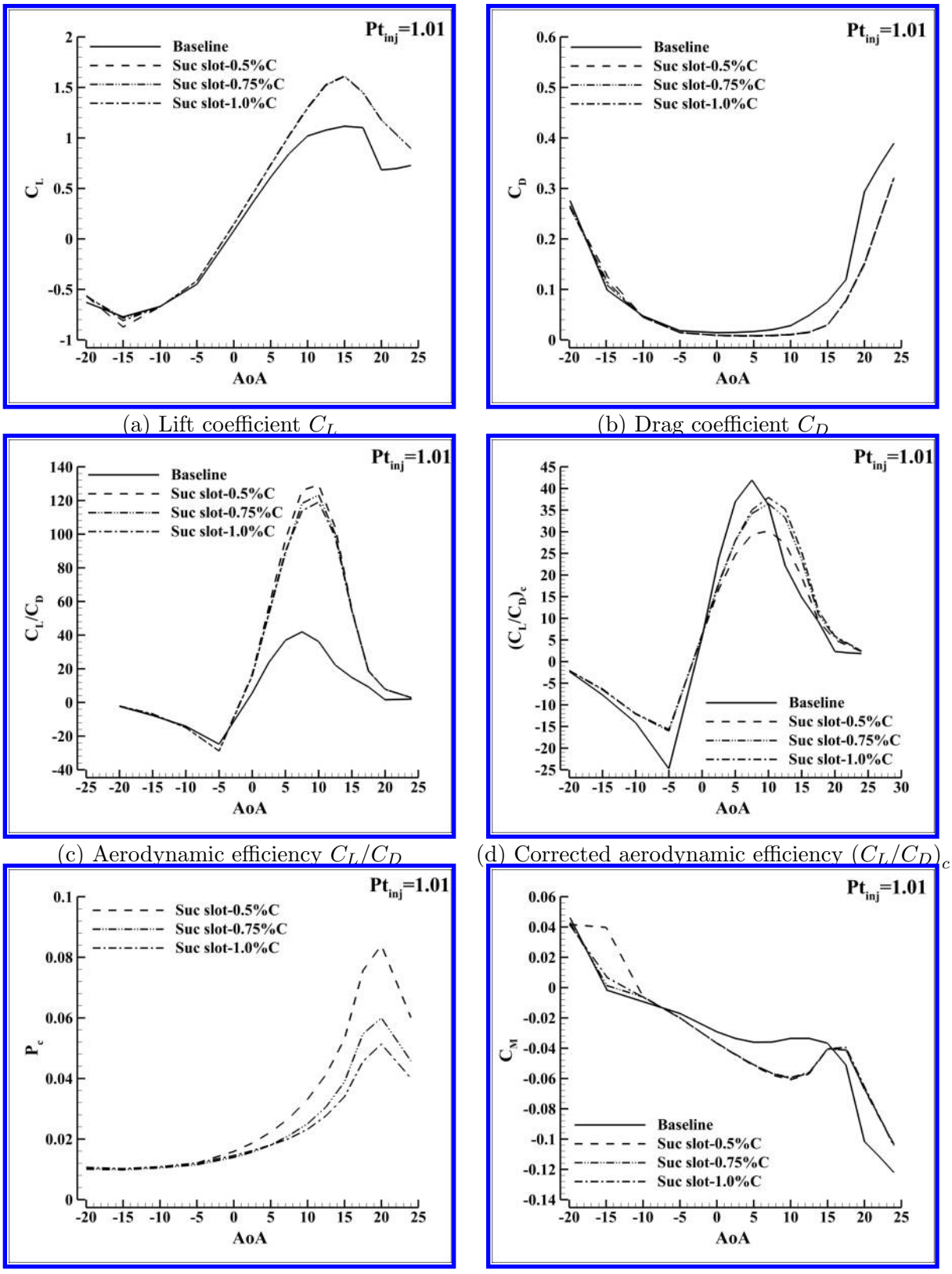

(a) Lift coefficient C_L

(b) Drag coefficient C_D

(c) Aerodynamic efficiency C_L/C_D

(d) Corrected aerodynamic efficiency $(C_L/C_D)_c$

(e) Power coefficient P_c

(f) Moment coefficient C_M

Figure 13: Aerodynamic coefficients of baseline and CFJ-S809 airfoils with suction slot-size variations for Pt_{inj}=1.01.

5.5 Injection Slot-size Study

Three injection slot-sizes of 0.5%C, 0.75%C, and 1.0%C are studied in this section. The suction slot-size of 1%C and location at 53%C is adopted from the studies in the previous sections. The injection total pressure is 1.01 for the injection slot-size of 0.5%C, and is varied slightly by 0.6% for the size of 0.75%C and 1.0%C to produce similar lift coefficients. Fig. 14 is the injection C_μ and Ptr of the three injection slot-sizes against AoA. Fig. 15 presents the aerodynamic coefficients of the CFJ-S809 airfoil for the three injection slot-sizes. With the similar lift enhancement, the slot-size of 0.75%C achieves the highest $(C_L/C_D)_c$ of 40.9, a 7.9% and 7.3% improvement respectively compared with the injection slot size of 0.5%C and 1.0%C. The corresponding power coefficient is 17% lower than the other two configurations at AoA of 10° for the peak aerodynamic efficiency.

A larger injection duct area increases the injection mass flow rate and reduces the required total pressure ratio for the micro-compressor actuator. Equation (7) indicates that the power coefficient is linearly determined by the mass flow rate and exponentially determined by the total pressure ratio. With the increased mass flow rate and reduced total pressure ratio, the power coefficient of injection slot-size of 0.75%C is decreased. However, further increasing the injection slot-size to 1.0%C does not have more reduction of power consumption. This is because when the injection slot size is too large, the injection velocity is too low. To achieve the same lift coefficient enhancement, a higher C_μ with larger mass flow rate is needed and it offsets the benefit of the low total pressure ratio. In other words, there is an optimum injection slot-size, below which a larger injection slot size is preferred. In conclusion, the injection slot-size of 0.75%C is adopted as the optimum for the next studies.

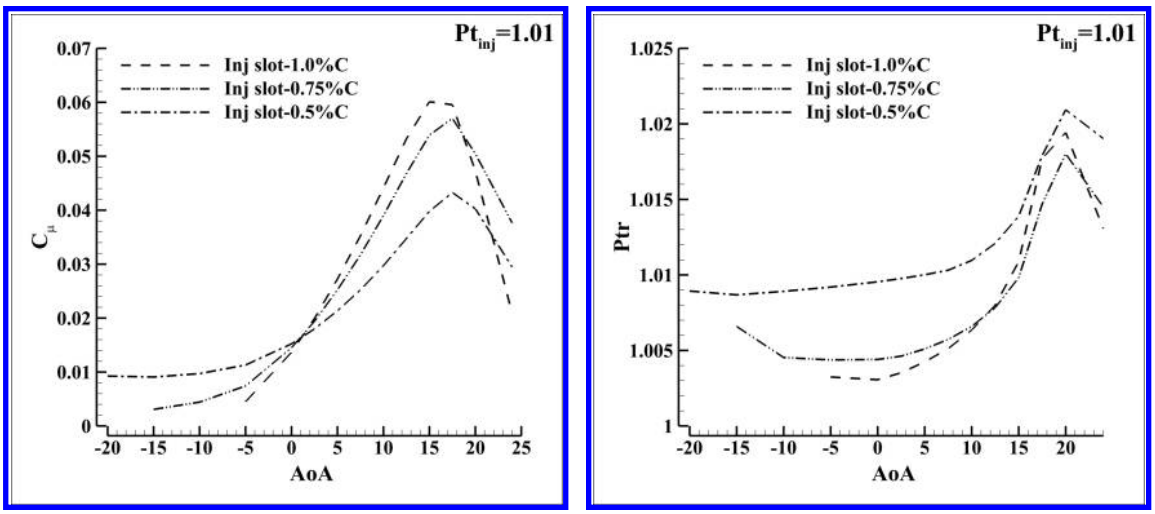

(a) Momentum coefficient C_μ (b) CFJ Total pressure ratio Ptr

Figure 14: C_μ and Ptr variations with AoA for injection slot-size studies.

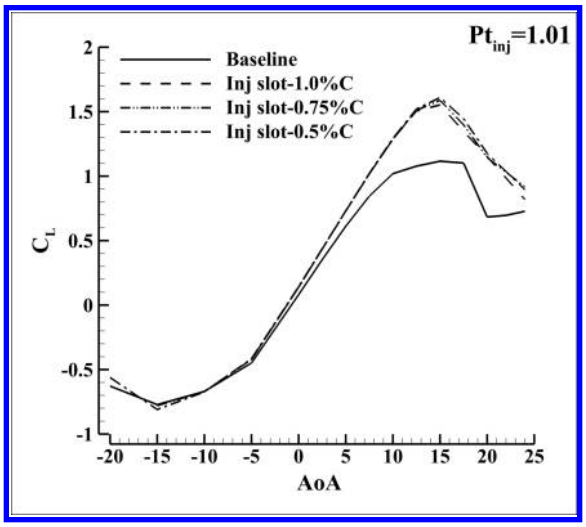

(a) Lift coefficient C_L

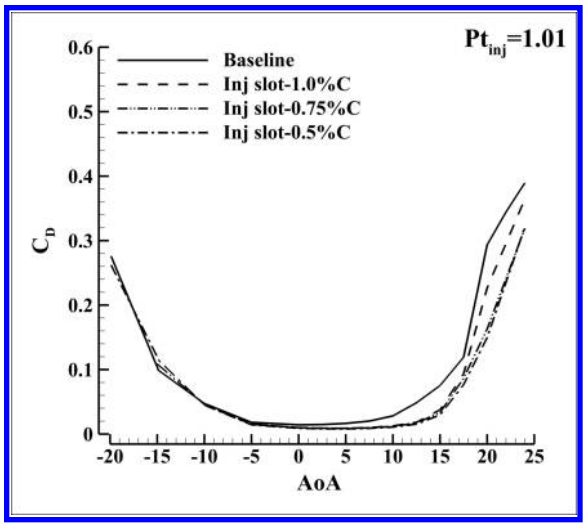

(b) Drag coefficient C_D

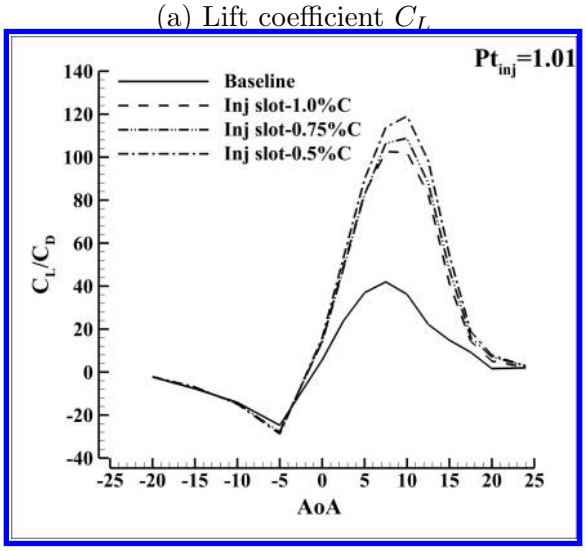

(c) Aerodynamic efficiency C_L/C_D

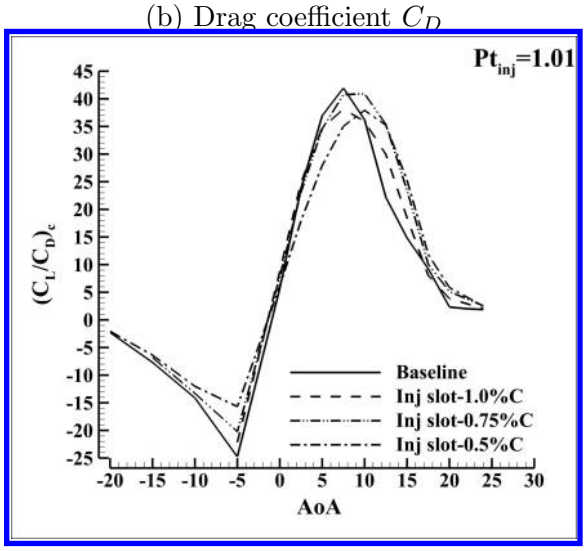

(d) Corrected aerodynamic efficiency $(C_L/C_D)_c$

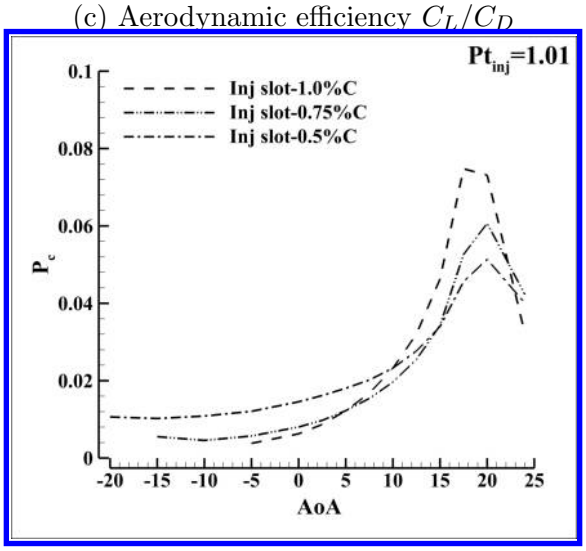

(e) Power coefficient P_c

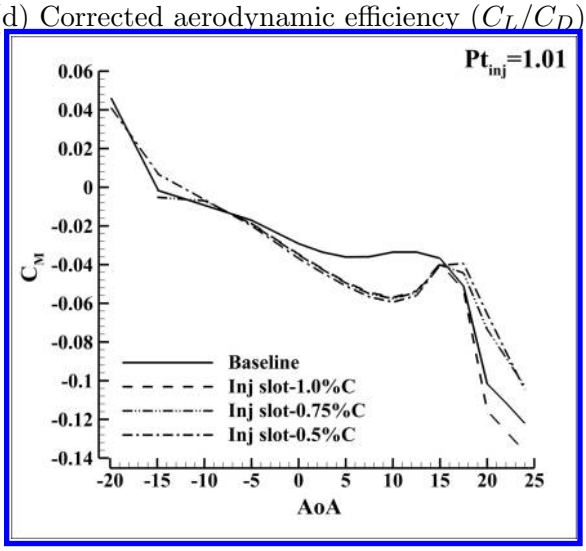

(f) Moment coefficient C_M

Figure 15: Aerodynamic coefficients of baseline and CFJ-S809 airfoils with injection slot-size variations for Pt_{inj}=1.01.

5.6 Injection Location Study

Three injection locations are studied in this section at 2%C, 3%C and 4%C. The injection and suction slot-sizes are fixed at 0.75%C and 1.0%C. The suction location is at 53%C. The injection total pressure is varied slightly by 0.5% for the three configurations to achieve the similar lift coefficient. Fig. 16 is the injection C_μ and Ptr distributions against the AoA for the three injection locations. Fig. 17 shows the aerodynamic coefficients of CFJ-S809 airfoil for the three injection locations. The power coefficients required by the three configurations varies with the different AoA. In the low AoA range from -20° to 2.5°, the 2%C injection location has the lowest power coefficient, which indicates such location works better in low AoA. As AoA is increased, the power coefficient of 2%C becomes higher than 3%C and 4%C due to the intensified flow separation inside the suction duct. As shown in Fig. 18, the separation bubble reduces the effective area of the suction duct, which increases the total pressure loss and power consumption of CFJ actuator. A very high peak $(C_L/C_D)_c$ of 41 is achieved for the injection locations of 3%C and 4%C at AoA of 10°, which is about the same as that of the baseline C_L/C_D. At the same AoA, the lift coefficient is increased by 27.5%. The peak $(C_L/C_D)_c$ of 2%C injection location is 5% lower. This indicates the 3%C and 4%C have a high energy efficiency at high AoA and is more capable to overcome turbine stall problem. Since the 3%C has a slightly higher C_{Lmax} than the 4%C, the 3%C injection location is adopted as the optimum injection location.

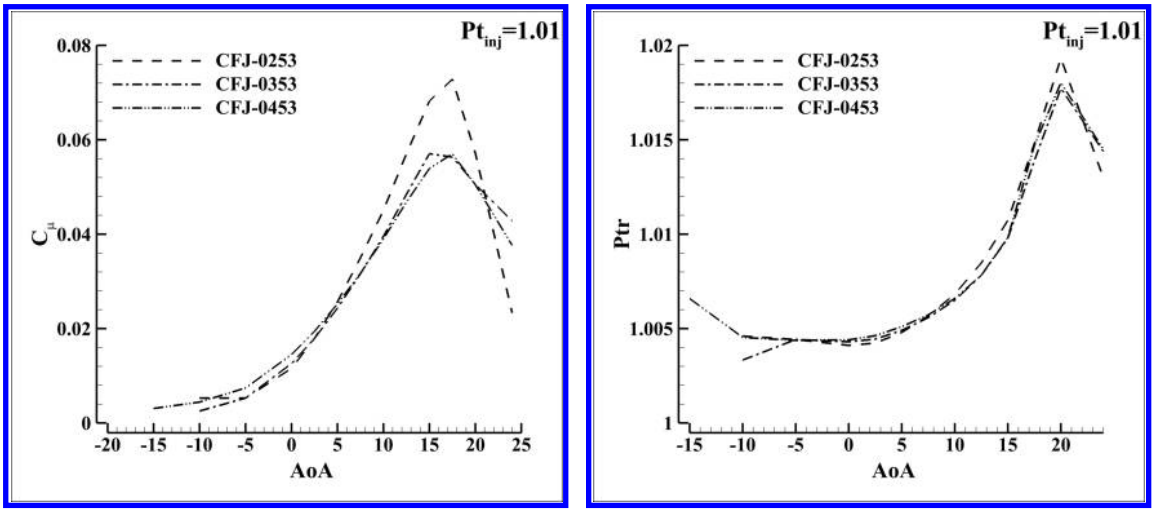

(a) Momentum coefficient C_μ (b) CFJ Total pressure ratio Ptr

Figure 16: C_μ and Ptr variations with AoA for injection location studies.

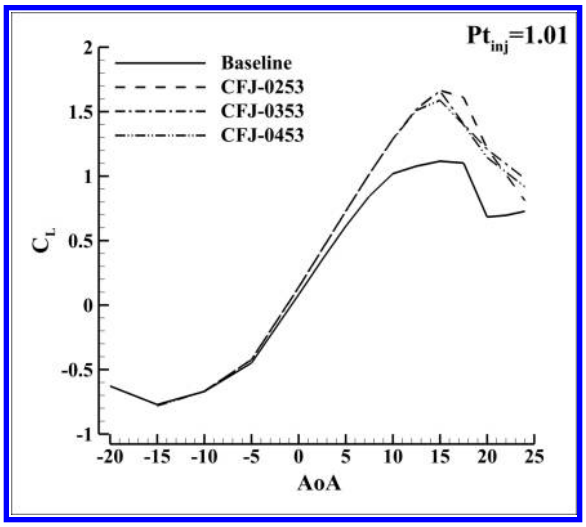

(a) Lift coefficient C_L

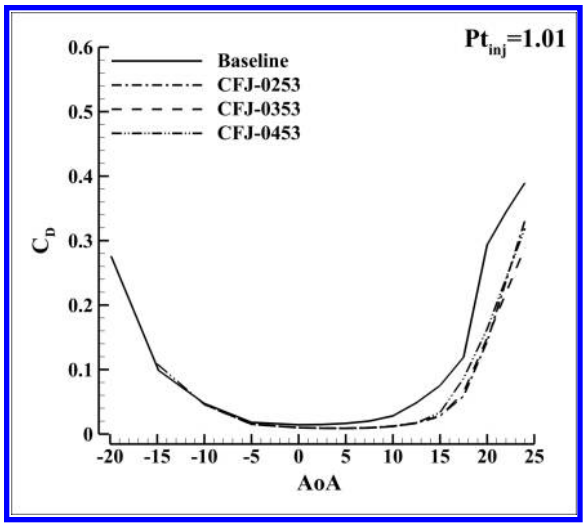

(b) Drag coefficient C_D

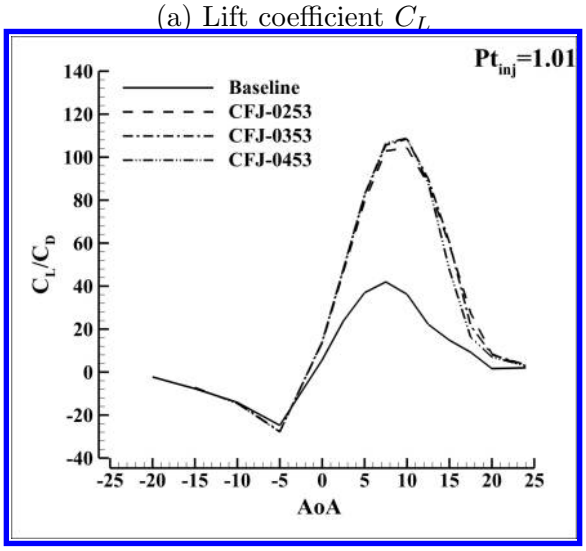

(c) Aerodynamic efficiency C_L/C_D

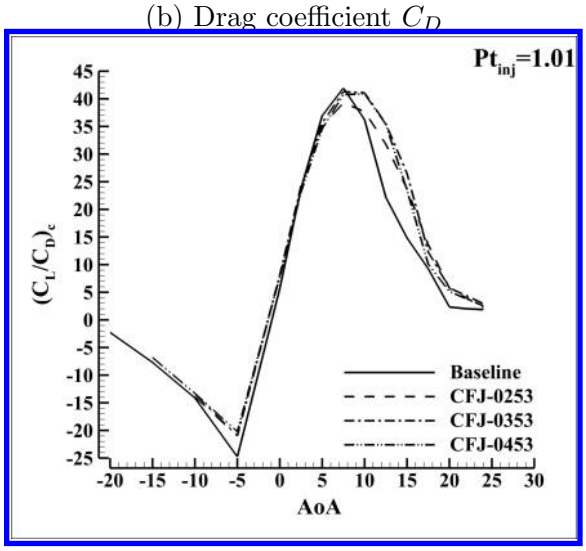

(d) Corrected aerodynamic efficiency $(C_L/C_D)_c$

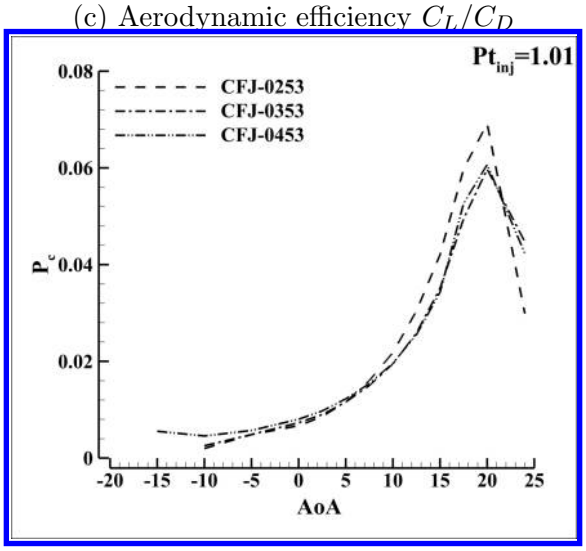

(e) Power coefficient P_c

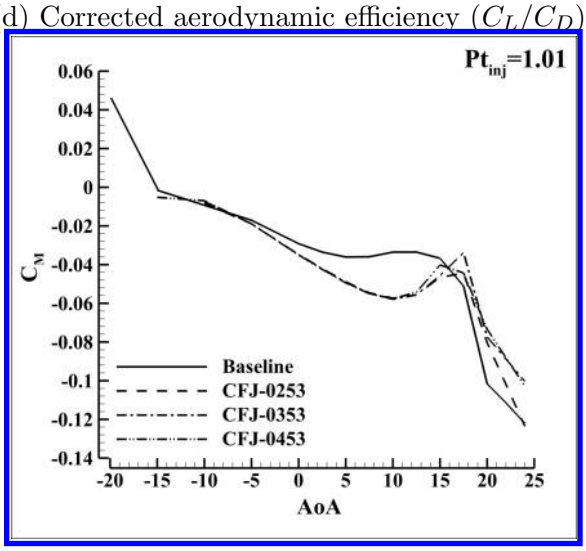

(f) Moment coefficient C_M

Figure 17: Aerodynamic coefficients of baseline and CFJ-S809 airfoils with injection location variations for Pt_{inj}=1.01.

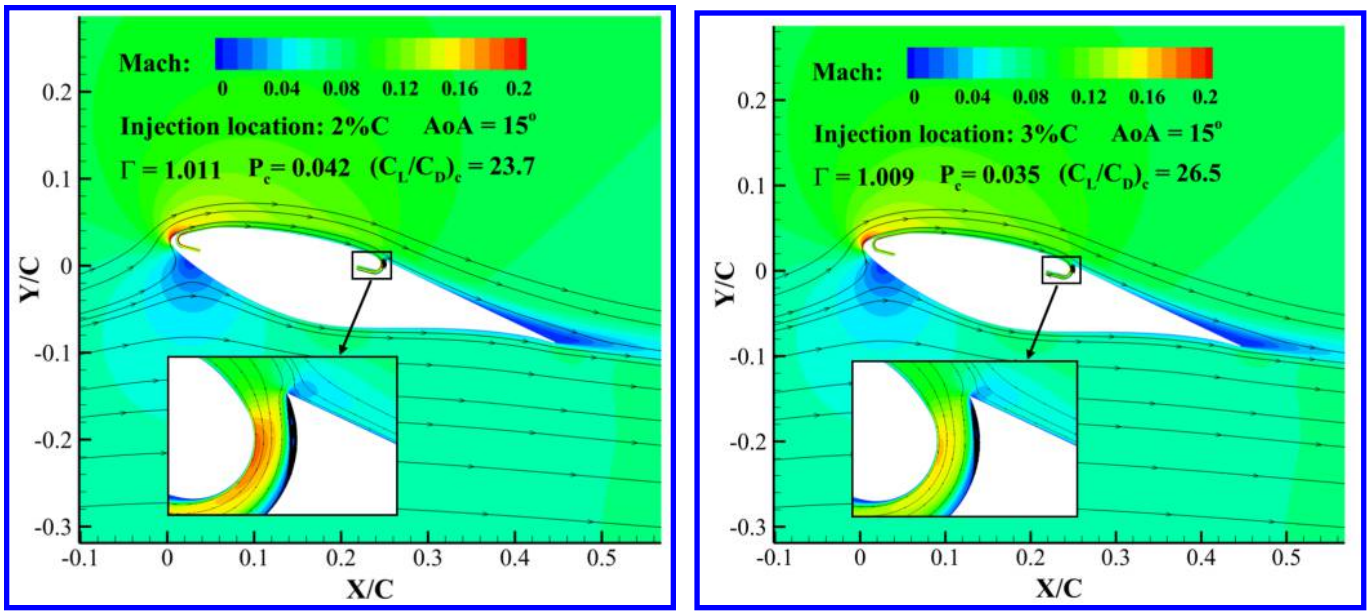

(a) CFJ-S809 airfoil with injection at 2%C (b) CFJ-S809 airfoil with injection at 3%C

Figure 18: Illustration of the flow separation inside suction duct of the CFJ-S809 airfoil at AoA of 15°

6 Conclusions

This paper applies Co-flow Jet (CFJ) active flow control (AFC) to the wind turbine S809 airfoil to optimize the CFJ-S809 airfoil with a significant lift coefficient increase at low energy expenditure. The effects of injection slot-size, injection slot location, suction slot-size and suction slot location are studied. The high fidelity in-house CFD code FASIP with two-equation k-ω shear stress transport (SST) turbulence model is utilized to better predict flow separation. The 2D Unsteady Reynolds averaged Navier-Stokes (URANS) equations are used for high angle of attack simulations to accurately capture flow unsteadiness. Steady state RANS is used for low angle of attack simulations. The numerical simulation of the baseline S809 airfoil is validated with the experiment. The predicted lift coefficient (C_L) and drag coefficient (C_D) achieve a good agreement with the experiment except a slight deviation at a very high or very low angle of attack (AoA) due to flow separation. The predicted airfoil surface pressure coefficient distribution (C_p) at various AoA also agrees well with experiments. The CFJ-S809 airfoil is simulated with three injection total pressure of CFJ actuator of 1.01, 1.02 and 1.03, which corresponds to the C_μ varying from 0.02 to 0.09 when the AoA is in the range of -20° and 25°. A small Pt_{inj} of 1.01 is able to increase C_{Lmax} over 45%. The suction location study indicates that suction slot located at the geometry inflection point at 53%C is the optimum due to it's efficiency and effectiveness to suppress airfoil separation at high AoA. The suction slot-size of 1.0%C is adopted since it decelerates the flow well with little flow separation inside the suction duct. For the injection slot-size, the 0.75%C slot minimizes the power coefficients by reducing the required injection total pressure, and therefore is the optimum. The injection location of 3%C is accepted as the final design due to it's better energy efficiency at high angle attack. Compared with the baseline S809 airfoil, the optimum configuration is able to increase C_{Lmax} by 42.3% with about the same $(C_L/C_D)_c$ as the baseline airfoil. Such performance enhancement will be able to significantly increase the wind turbine power output. An application of CFJ to 3D wind turbine blade is necessary to demonstrate the improvement.

7 Acknowledgment

The authors would like to acknowledge the computing resource provided by the Center for Computational Sciences at the University of Miami.

Disclosure: The University of Miami and Dr. Gecheng Zha may receive royalties for future commercialization of the intellectual property used in this study.

References

[1] R. Ramsay, M. Hoffman, and G. Gregorek, "Effects of grit roughness and pitch oscillations on the s809 airfoil," tech. rep., National Renewable Energy Lab., Golden, CO (United States), 1995.

[2] D. M. Somers, "Design and experimental results for the s809 airfoil," tech. rep., National Renewable Energy Lab., Golden, CO (United States), 1997.

[3] G. Wang, J. Walczak, B. Elhadidi, M. Glauser, and H. Higuchi, "Preliminary investigation of the active flow control benefits on wind turbine blades," in *6th AIAA Theoretical Fluid Mechanics Conference*, pp. AIAA 2011–3611, Honolulu, Hawaii, 27 June 2011 - 30 June 2011.

[4] T.-J. Kang and W.-G. Park, "Numerical investigation of active control for an s809 wind turbine airfoil," *International Journal of Precision Engineering and Manufacturing*, vol. 14, no. 6, pp. 1037–1041, 2013.

[5] V. Maldonado and S. Gupta, "Active flow control of a low reynolds number s809 wind turbine blade model under dynamic pitching maneuvers," *Open Journal of Fluid Dynamics*, vol. 7, no. 02, p. 178, 2017.

[6] M. Gul, O. Uzol, and I. Akmandor, "An experimental study on active flow control using synthetic jet actuators over s809 airfoil," in *Journal of Physics: Conference Series*, vol. 524, p. 012101, IOP Publishing, 2014.

[7] G.-C. Zha, B. F Carroll, C. D. Paxton, C. A. Conley, and A. Wells, "High-performance airfoil using coflow jet flow control," *AIAA journal*, vol. 45, no. 8, pp. 2087–2090, 2007.

[8] A. Lefebvre, B. Dano, W. Bartow, M. Fronzo, and G. Zha, "Performance and energy expenditure of coflow jet airfoil with variation of mach number," *Journal of Aircraft*, vol. 53, no. 6, pp. 1757–1767, 2016.

[9] G. Zha, W. Gao, and C.D. Paxton, "Jet Effects on Co-Flow Jet Airfoil Performance," *AIAA Journal*, vol. 45, pp. 1222–1231, 2007.

[10] G.-C. Zha, C. Paxton, A. Conley, A. Wells, nd B. Carroll, "Effect of Injection Slot Size on High Performance Co-Flow Jet Airfoil," *AIAA Journal of Aircraft*, vol. 43, pp. 987–995, 2006.

[11] B. Wang, B. Haddoukessouni, J. Levy, and G.-C. Zha, "Numerical investigations of injection-slot-size effect on the performance of coflow jet airfoils," *Journal of Aircraft*, vol. 45, no. 6, pp. 2084–2091, 2008.

[12] B. P. E. Dano, D. Kirk, and G.-C. Zha, "Experimental Investigation of Jet Mixing Mechanism of Co-Flow Jet Airfoil." AIAA-2010-4421, 5th AIAA Flow Control Conference, Chicago, IL, 28 Jun - 1 Jul 2010.

[13] B. Dano, G. Zha, and M. Castillo, "Experimental study of co-flow jet airfoil performance enhancement using discreet jets." AIAA Paper 2011-941, 49th AIAA Aerospace Sciences Meeting including the New Horizons Forum and Aerospace Exposition, Orlando, Florida, 04 January 2011 - 07 January 2011.

[14] Lefebvre, A. and Zha, G.-C. , "Design of High Wing Loading Compact Electric Airplane Utilizing Co-Flow Jet Flow Control." AIAA Paper 2015-0772, AIAA SciTech2015: 53nd Aerospace Sciences Meeting, Kissimmee, FL, 5-9 Jan 2015.

[15] Liu, Z.-X. and Zha, G.-C., "Transonic Airfoil Performance Enhancement Using Co-Flow Jet Active Flow Control." AIAA Paper 2016-3066, AIAA Aviation, Washington, D.C., June 13-17 2016.

[16] Lefebvre, A. and Zha, G.-C., "Trade Study of 3D Co-Flow Jet Wing for Cruise Performance." AIAA Paper 2016-0570, AIAA SCITECH2016, AIAA Aerospace Science Meeting, San Diego, CA, 4-8 January 2016.

[17] G. Zha, Y. Yang, Y. Ren, and B. McBreen, "Super-lift and thrusting airfoil of coflow jet actuated by micro-compressors," in *2018 Flow Control Conference, AIAA 2018-3061, Atlanta, Georgia, June 25-29*, 2018.

[18] J. Zhang, K. Xu, Y. Yang, Y. Ren, P. Patel, and G. Zha, "Aircraft control surfaces using co-flow jet active flow control airfoil." AIAA Paper 2018-3067, 2018 Applied Aerodynamics Conference, Atlanta, Georgia, June 25-29, 2018.

[19] K. Xu, J. Zhang, and G. Zha, "Drag minimization of co-flow jet control surfaces at cruise conditions." AIAA 2019-1848, AIAA Scitech 2019 Forum, San Diego, California, 7-11 January 2019.

[20] K. Xu and G. Zha, "High control authority 3d aircraft control surfaces using co-flow jet," in *AIAA Aviation 2019 Forum*, pp. AIAA Paper 2019–3168, 17-21 June 2019, Dallas, Texas.

[21] K. Xu, Y. Ren, and G. Zha, "Numerical investigation of nasa hump using co-flow jet for separation control." AIAA Paper will be presented in 2020 AIAA SciTech Forum, Orlando, Florida, 6C10 January, 2020.

[22] K. Xu and G. Zha, "Mitigation of serpentine duct flow distortion using coflow jet active flow control." submitted to 2020 AIAA Aviation and Aeronautics Forum and Exposition, 15-19 June 2020.

[23] H.-Y. Xu, C.-L. Qiao, and Z.-Y. Ye, "Dynamic stall control on the wind turbine airfoil via a co-flow jet," *Energies*, vol. 9, no. 6, p. 429, 2016.

[24] H. Xu, S. Xing, and Z. Ye, "Numerical simulation of the effect of a co-flow jet on the wind turbine airfoil aerodynamic characteristics," *Procedia Engineering*, vol. 126, pp. 706–710, 2015.

[25] P. Patel and G. Zha, "Improved delayed detached eddy simulation of separated flow," in *AIAA Aviation 2020 Forum*, June 2020.

[26] Y.-Q. Shen, G.-C. Zha, and B.-Y. Wang, "Improvement of Stability and Accuracy of Implicit WENO Scheme ," *AIAA Journal*, vol. 47, pp. 331–344, 2009.

[27] Shen, Y.-Q. and Zha, G.-C. and Chen, X.-Y., " High Order Conservative Differencing for Viscous Terms and the Application to Vortex-Induced Vibration Flows," *Journal of Computational Physics*, vol. 228(2), pp. 8283–8300, 2009.

[28] Shen, Y.-Q. and Zha, G.-C. , " Improvement of the WENO Scheme Smoothness Estimator," *International Journal for Numerical Methods in Fluids*, vol. DOI:10.1002/fld.2186, 2009.

[29] G.-C. Zha and E. Bilgen, "Numerical study of three-dimensional flows using unfactored upwind-relaxation sweeping algorithm," *Journal of Computational Physics*, vol. 125, no. 2, pp. 425–433, 1996.

[30] B. Wang, Z. Hu, and G.-C. Zha, "General subdomain boundary mapping procedure for structured grid implicit cfd parallel computation," *Journal of Aerospace Computing, Information, and Communication*, vol. 5, no. 11, pp. 425–447, 2008.

[31] B. Wang and G.-C. Zha, "Detached-eddy simulation of a coflow jet airfoil at high angle of attack," *Journal of aircraft*, vol. 48, no. 5, pp. 1495–1502, 2011.

[32] Y. Yang and G. Zha, "Super-lift coefficient of active flow control airfoil: What is the limit?." AIAA Paper 2017-1693, AIAA SCITECH2017, 55th AIAA Aerospace Science Meeting, Grapevine, January 9-13 2017.

[33] Im, H.-S. and Zha, G.-C. and Dano, B. P. E., "Large Eddy Simulation of Coflow Jet Airfoil at High Angle of Attack," *Journal of Fluid Engineering, vol. 136(2), p. 021101*, 2014.